Localized waves with spherical harmonic symmetries

M. S. Mills,[1,*] G. A. Siviloglou,[2] N. Efremidis,[3] T. Graf,[4] E. M. Wright,[4] J. V. Moloney,[4] and D. N. Christodoulides[1]

[1]*CREOL School of Optics, University of Central Florida, Orlando, Florida 32816, USA*

[2]*MIT-Harvard Center for Ultracold Atoms, Research Laboratory of Electronics, and Department of Physics,*
Massachusetts Institute of Technology, Cambridge, Massachusetts 02139, USA

[3]*Department of Applied Mathematics, University of Crete, Heraklion 71409, Crete, Greece*

[4]*College of Optical Sciences, The University of Arizona, Tuscon, Arizona 85721, USA*

We introduce a class of propagation invariant spatiotemporal optical wave packets with spherical harmonic symmetries in their field configurations. The evolution of these light orbitals is considered theoretically in anomalously dispersive media, and their spinning dynamics are analyzed in terms of their corresponding energy flows. Similarly, localized waves generated via spherical superposition from Archimedean and Platonic solids in $\vec{k}$-ω space are investigated in this work.

PACS number(s): 42.25.Fx, 42.25.Hz, 42.25.Bs

I. INTRODUCTION

The evolution dynamics of propagation invariant optical fields have recently attracted considerable attention within the optics community [1–10]. Undoubtedly, this area grew in earnest after the first demonstration of optical Bessel beams by Durnin *et al.* in 1987 [1,2]. Since then, other groups of two-dimensional nondiffracting beams have been reported in the literature [3–8]. In general, diffraction-free beams can maintain their localized intensity features over several Rayleigh lengths until aperture diffraction effects come into play. Quite recently, accelerating nondiffracting Airy wave packets have also been observed experimentally in one- and two-dimensional configurations [8]. By now, such field arrangements have been systematically used in several diverse disciplines ranging from microparticle manipulation to plasma channel generation to nonlinear optics [11–15].

In the spatiotemporal domain, the prospect for localized waves that can simultaneously negotiate both dispersion and diffraction effects in the bulk has been actively pursued by several research groups in both the linear and nonlinear regimes [16–18]. In general, an optical wave packet propagating in a homogeneous dielectric medium will expand because of diffraction effects while at the same time its temporal profile will broaden because of dispersion. In the linear domain, specific wave solutions are known to exist under normally and anomalously dispersive conditions. For normal dispersion, these solutions exhibit an *X*-wave structure [5,19]—a direct outcome of the bidispersive nature of the underlying wave equation [6]. In the anomalous domain, spherical *O* waves [18,20] are allowed and Bessel-*X* pulses are possible under specific conditions [21]; however, this constraint on the sign of dispersion can be relaxed either under nonparaxial conditions or when the velocity of the localized wave is largely different from the medium's linear group velocity. In fact, not only has it been shown that a crossover from *X* to *O* waves can occur in a dispersive medium, but localized waves that fit neither category are also possible [22,23]. Recently, three-dimensional (3D) Airy-Bessel bullets that are impervious to both dispersion

and diffraction have been suggested [9] and successfully demonstrated in dispersive media [24]. This versatile class of optical wave packets was made possible by exploiting the fact that nonspreading Airy waves can exist even in one dimension (1D). This class of Airy-Bessel bullets is possible irrespective of the dispersion properties of the material itself.

The quest for such spatiotemporal entities is clearly intertwined with experimental capabilities of simultaneously shaping their $\vec{k}$-ω spectra. Over the years, various techniques have been developed to address these needs in either the spatial or temporal domain [25,26]. Lately, methods that allow for the generation of quasi-nondiffracting light beams with complex transverse shapes have been suggested [27]. Further progress in this area may pave the way towards the generation of other exotic space-time waves with unique properties tailored for particular light-matter interaction processes [28].

In this paper, we present a class of spatiotemporal wave fronts that is possible under anomalously dispersive conditions. Depending on their angular momentum numbers, these wave packets exhibit polar and azimuthal symmetries akin to those encountered in the quantum-mechanical wave functions of a hydrogen atom. The dynamics of such states when they are apodized are analytically studied along with their associated energy flows. Other types of localized waves generated through a spherical superposition from Archimedean and Platonic solids in $\vec{k}$-ω space are also investigated in this work. The possibility of spinning localized waves is considered and the prospect for their realization is discussed.

II. PROBLEM FORMULATION AND ANALYSIS

In general, the primary electric field associated with a wave packet can be expressed through a slowly varying envelope via $\vec{E}(\vec{r},t) = \hat{u}\psi(\vec{r},t) \exp[i(k_0 z - \omega_0 t)]$, where ω_0 is the carrier angular frequency, $k_0 = \omega_0 n(\omega_0)/c$ is the wave number evaluated at ω_0, and $n(\omega_0)$ is the refractive index. The spatiotemporal evolution of the envelope, $\psi(\vec{r},t)$, under the combined action of diffraction and group-velocity dispersion is known to obey the following evolution equation:

$$i\frac{\partial \psi}{\partial z} + \frac{1}{2k}\left(\frac{\partial^2 \psi}{\partial x^2} + \frac{\partial^2 \psi}{\partial y^2}\right) - \frac{k_2}{2}\frac{\partial^2 \psi}{\partial \tau^2} = 0, \qquad (1)$$

*millsms@knights.ucf.edu

where in (1), $\tau = t - z/v_g$ is a time coordinate frame moving at the wave's group speed, v_g, and $k_2 = \partial^2 k/\partial \omega^2$ represents the dispersive coefficient of the homogeneous medium again evaluated at ω_0. The material is anomalously dispersive if $k_2 < 0$ and is normal if $k_2 > 0$. The transverse spatial operators in (1) account for diffraction effects, while the temporal operator accounts for the action of dispersion. Equation (1) can be judiciously scaled by normalizing the independent variables involved in such a way that the diffraction length $L_{\text{diff}} = 2kd^2$ is equal to the corresponding dispersion length $L_{\text{disp}} = \tau_0^2/|k_2|$, i.e., $L_{\text{disp}} = L_{\text{diff}}$. Here, d is an arbitrary length scale and τ_0 is associated with the pulse width of the wave packet. From this point on, the material dispersion is taken to be anomalous in our analysis. Under these assumptions, Eq. (1) takes the form

$$i\frac{\partial \psi}{\partial Z} + \frac{\partial^2 \psi}{\partial X^2} + \frac{\partial^2 \psi}{\partial Y^2} + \frac{\partial^2 \psi}{\partial T^2} = 0, \qquad (2)$$

where in (2) we have employed the set of normalized coordinates and variables $X = x/d$, $Y = y/d$, $Z = z/(2kd^2)$, and $T = \tau/\tau_0$.

The aforementioned spatiotemporal wave packets can be studied experimentally in anomalously dispersive bulk media such as silica glass. Silica, at $\lambda_0 = 1550$ nm, exhibits a dispersive coefficient of $k_2 = -2.8 \times 10^{-2}$ ps^2/m. For this example, such a dispersion-diffraction equalization ($L_{\text{diff}} = L_{\text{disp}} = 5.7$ cm) is possible provided that the wave packet generated from a transform limited femtosecond laser has the parameters $\tau_0 = 40$ fs and $d = 100$ μm.

In what follows, we will derive the electromagnetic equations describing the internal power flow associated with a spatiotemporal wave packet as a result of dispersion and diffraction. This is necessary in order to comprehend the underlying dynamics in such systems. With this in mind, we employ a perturbative approach, valid within the slowly varying envelope approximation and paraxial diffraction optics. We start our analysis by writing the electric field as a superposition of plane waves centered around a carrier frequency, ω_0. Without any loss of generality, the primary electric-field component is taken here to be $\hat{x}$ polarized. In this case

$$\vec{E} = \hat{x}\iiint F_0(\omega - \omega_0; k_x, k_y)$$
$$\times \exp[i(\vec{k} \cdot \vec{r} - \omega t)]d\omega\, dk_x\, dk_y. \qquad (3)$$

This same field can also be expressed in terms of a slowly varying envelope ψ, i.e., $\vec{E}(\vec{r},t) = \hat{x}\psi(\vec{r},t)\exp[i(k_0 z - \omega_0 t)]$. Given that $k_z \approx k - (k_x^2 + k_y^2)/(2k)$ and that the wave number can be expanded in a Taylor series around ω_0, $k \approx k_0 + k_1\Omega + k_2\Omega^2/2$ (where $\Omega = \omega - \omega_0$), one finds

$$\psi(\vec{r},t) = \iiint F_0(\Omega; k_x, k_y)\exp[i(k_x x + k_y y)]$$
$$\times \exp\left[-\frac{i}{2k}(k_x^2 + k_y^2)z\right]\exp\left[i\left(k_1\Omega + k_2\frac{\Omega^2}{2}\right)z\right]$$
$$\times \exp[-i\Omega\tau]\,d\Omega\, dk_x\, dk_y, \qquad (4)$$

where $v_g^{-1} = k_1$. The associated longitudinal component of the electric field can be then obtained from $\nabla \cdot \vec{E} = 0$, leading to

a total (corrected to first order) electric field that is given by

$$\vec{E} = \left(\hat{x}\psi + \hat{z}\frac{i}{k_0}\frac{\partial \psi}{\partial x}\right)\exp[i(k_0 z - \omega_0 t)]. \qquad (5)$$

The primary magnetic field of this wave packet can be obtained from the electric field through the material intrinsic impedance $\eta(\omega) = \eta_0/n(\omega)$, where $\eta_0 = \sqrt{(\mu_0/\epsilon_0)}$. Therefore

$$\vec{H} = \hat{y}\iiint \frac{F_0(\Omega; k_x, k_y)}{\eta(\omega)}\exp[i(\vec{k} \cdot \vec{r} - \omega t)]d\omega\, dk_x\, dk_y$$
$$= \hat{y}\iiint \frac{F_0(\Omega; k_x, k_y)}{\eta_0}(n_0 + n_1\Omega)\exp[i(k_x x + k_y y)]$$
$$\times \exp\left[-\frac{i}{2k}(k_x^2 + k_y^2)z\right]\exp\left[i\left(k_1\Omega + k_2\frac{\Omega^2}{2}\right)z\right]$$
$$\times \exp[-i\Omega\tau]d\Omega\, dk_x\, dk_y\exp[i(k_0 z - \omega_0 t)]$$
$$= \frac{1}{\eta_0}\hat{y}\left[n_0\psi + in_1\frac{\partial \psi}{\partial \tau}\right]\exp[i(k_0 z - \omega_0 t)], \qquad (6)$$

where in (6) $n(\omega) = n(\omega_0 + \Omega)$ and $n_1 = \partial n/\partial \omega$ at ω_0. These coefficients can, in principle, be evaluated from the corresponding Sellmeier equation associated with the dispersive medium. From $\nabla \cdot \vec{H} = 0$, one can determine (to first order) the longitudinal component of the magnetic field. The total magnetic field is found to be

$$\vec{H} = \left(\frac{1}{\eta_0}\hat{y}\left[n_0\psi + in_1\frac{\partial \psi}{\partial \tau}\right] + \hat{z}i\frac{n_0}{k_0\eta_0}\frac{\partial \psi}{\partial y}\right)$$
$$\times \exp[i(k_0 z - \omega_0 t)]. \qquad (7)$$

The power flow within the spatiotemporal wave packet can now be established from Eqs. (5) and (7), i.e.,

$$\overrightarrow{S_{\text{av}}} = \hat{z}\frac{n_0}{2\eta_0}|\psi|^2 - i\hat{z}\frac{n_1}{4\eta_0}\left[\psi\frac{\partial \psi^\star}{\partial \tau} - \psi^\star\frac{\partial \psi}{\partial \tau}\right]$$
$$+ \frac{in_0}{4k_0\eta_0}[\psi\nabla_\perp\psi^\star - \psi^\star\nabla_\perp\psi], \qquad (8)$$

where $\nabla_\perp = (\partial^2/\partial x^2)\hat{x} + (\partial^2/\partial y^2)\hat{y}$. The last two terms in Eq. (8) correspond to the relative power flow corrections. The second term along $\hat{z}$ is due to temporal effects, while the $\nabla_\perp$ component accounts for the energy transport because of transverse effects. We note here that the first term in (8) represents the dominant contribution to the power flow. Equation (8) can now be expressed in normalized units as follows:

$$\overrightarrow{S_{\text{av}}} = \overrightarrow{S_0} + \overrightarrow{S_r}, \qquad \overrightarrow{S_0} = \hat{z}\frac{n_0}{2\eta_0}|\psi|^2,$$
$$\overrightarrow{S_r} = -i\hat{z}\frac{n_1}{4\eta_0\tau_0}\left[\psi\frac{\partial \psi^\star}{\partial T} - \psi^\star\frac{\partial \psi}{\partial T}\right]$$
$$+ \frac{in_0}{4k_0\eta_0 d}[\psi\tilde{\nabla}_\perp\psi^\star - \psi^\star\tilde{\nabla}_\perp\psi], \qquad (9)$$

where the transverse $\tilde{\nabla}_\perp$ operator involves the X and Y scaled coordinates.

III. LOCALIZED WAVES WITH SPHERICAL HARMONIC SYMMETRIES

Propagation invariant solutions to Eq. (2) can be directly obtained via separation of variables in

spatiotemporal spherical coordinates R, θ, ϕ, where $R^2 = X^2 + Y^2 + T^2$. To do so, we write the solution as $\psi = \psi_0 G(R) P(\theta) \exp(im\phi) \exp(-i\alpha^2 Z)$. Direct substitution of this latter form into (2) gives the following equations:

$$\frac{d}{d\theta}\left[\sin\theta \frac{dP}{d\theta}\right] + \sin\theta\left[\ell(\ell+1) - \frac{m^2}{\sin^2\theta}\right]P = 0, \quad (10)$$

$$R^2 \frac{d^2 G}{dR^2} + 2R\frac{dG}{dR} + [\alpha^2 R^2 - \ell(\ell+1)]G = 0. \quad (11)$$

It is interesting to note that a similar polar-azimuthal differential equation [Eq. (10)] is encountered in the analysis of hydrogen quantum orbitals. The solutions to the Legendre equation (10) can be obtained in terms of the associated Legendre polynomials $P_\ell^m(\gamma)$ of degree ℓ and order m, where $\gamma = \cos\theta$. Equation (11), on the other hand, has spherical Bessel function solutions $j_\ell(\alpha R) = \sqrt{\pi/(2\alpha R)}J_{\ell+1/2}(\alpha R)$ which can be expressed in terms of elementary functions since ℓ belongs to the natural numbers. Therefore, invariant solutions to Eq. (2) are given by

$$\psi_B = \sqrt{2\pi}\psi_0 j_\ell(\alpha R) P_\ell^m(\cos\theta)\exp[im\phi]e^{-i\alpha^2 Z}, \quad (12)$$

where ψ_0 is a constant amplitude. Akin to the two angular momentum quantum numbers in the hydrogen atom, the integer index ℓ takes values from the set $\ell = 0, 1, 2, \ldots$, while the integer order m is constrained in the range $|m| \leqslant \ell$. We note that, in general, these solutions depend on how the spherical coordinate system is oriented with respect to the X, Y, T axes. If, for example, the T coordinate coincides with the spherical polar axis, then $\theta = \arctan(\sqrt{X^2 + Y^2}/T)$ and $\phi = \arctan(Y/X)$. In principle, however, the spherical polar axis can be oriented in any direction (for example, along X or Y). This choice has an important effect on the associated relative internal power flows $\overrightarrow{S_r}$. In this case, the vorticity arising from the term $\exp[im\phi]$ takes on a whole new physical meaning in space-time.

The simplest possible member in this family of solutions given by Eq. (12) is obtained when $\ell = m = 0$. This lowest state has no internal spin and because it is like hydrogen's "s" orbital we call it an s wave. An isointensity contour plot of this wave packet is depicted in Fig. 1(a). This wave is evidently spherical and its field follows a $j_0(R) \propto \sin R/R$ radial distribution. As a result, its intensity structure involves concentric spherical shells as shown in Fig 1(b), which
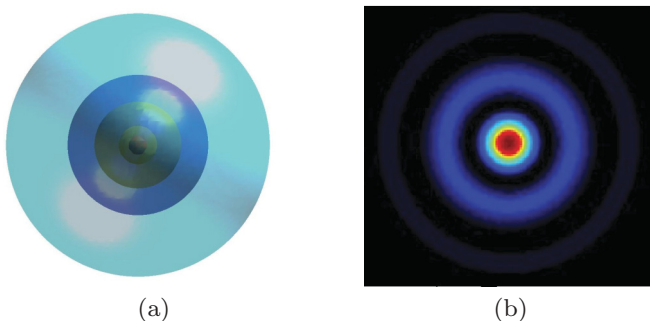

FIG. 1. (Color online) (a) Intensity isosurface plots of an $\ell = m = 0$ localized wave. (b) Intensity cross section reveals the $j_0(R) \propto \sin R/R$ profile of this "s" state.
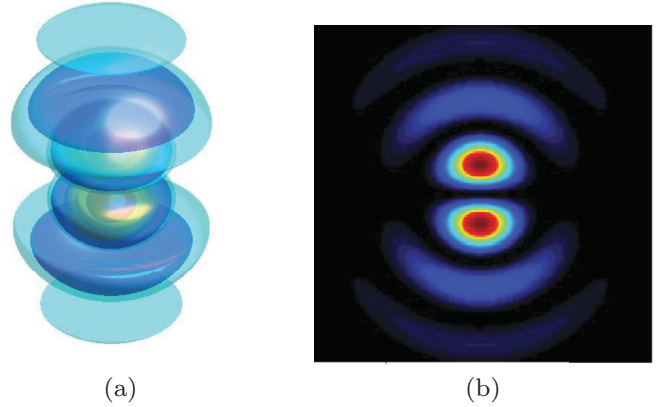

FIG. 2. (Color online) (a) Intensity isosurface plots of an $\ell = 1$, $m = 0$ localized wave. (b) Intensity cross section of "p" shell for $X = 0$.

represents a cross section of this localized wave in the Y-T plane. We note that this specific s member is identical to the so-called "o wave" previously obtained in other studies [18,20]. Figure 2(a), on the other hand, shows an isointensity plot of a space-time localized wave when $\ell = 1$, $m = 0$, in which case it corresponds to a p_T-like orbital. The structure of this solution is no longer spherical and lacks spin since $m = 0$. Note that this same state can be arbitrarily oriented in the X, Y, T system. A cross section of this solution at $X = 0$ [Fig. 2(b)] reveals the finer structure in its field distribution.

As in the case of s waves these solutions exhibit infinitely many rings in sharp contrast to the quantum orbitals of hydrogen. This is because in our case the Coulombic potential is not involved. Similarly, p_x and p_y waves can be generated from the same "quantum" numbers $\ell = 1$, $m = 0$. By further increasing the ℓ number, localized waves of higher symmetries can be generated similar to the ones depicted in Fig. 3. In particular, when $\ell = 2$ and $m = 0$ [Fig. 3(a)] the propagation invariant wave packet corresponds to the d_{TT} group (d orbitals). Similarly, an f-symmetric spatiotemporal wave packet with $\ell = 3$, $m = 0$ is shown in Fig. 3(b).

If we assume a state with finite spin ($m \neq 0$), an internal power flow will be present in the wave packet arising from its $\exp[im\phi]$ dependence. Figure 4(a) depicts the isointensity plot of an $\ell = m = +2$ wave, while Fig. 4(b) shows its corresponding internal power circulation, $\overrightarrow{S_r}$, which happens in this case to be clockwise. As would be anticipated, for $m = -2$ we obtain the same isointensity plot, while the power circulation is counterclockwise [Fig. 4(c)].

This leads to the possibility of realizing superpositions (e.g., $\exp[+im\phi] + \exp[-im\phi]$) of spatiotemporal entities that share the same ℓ number and opposite "spin" numbers, m. If, for example, $\ell = 2$ and $m = \pm 1$, the wave packet will have a fourfold symmetry [Fig. 5(a)] and it will be d_{YT} symmetric. On the other hand, a d_{XY}-symmetric wave function will be similar to the one shown Fig. 5(b) for characteristic indices $\ell = 2$ and $m = \pm 2$.

In principle, a superposition of two such spatiotemporal localized waves that have identical "quantum numbers," ℓ and m, but with slightly different propagation constants ($\alpha_1 \approx \alpha_2$) can lead to a "breathing" wave packet. If, on the other hand,

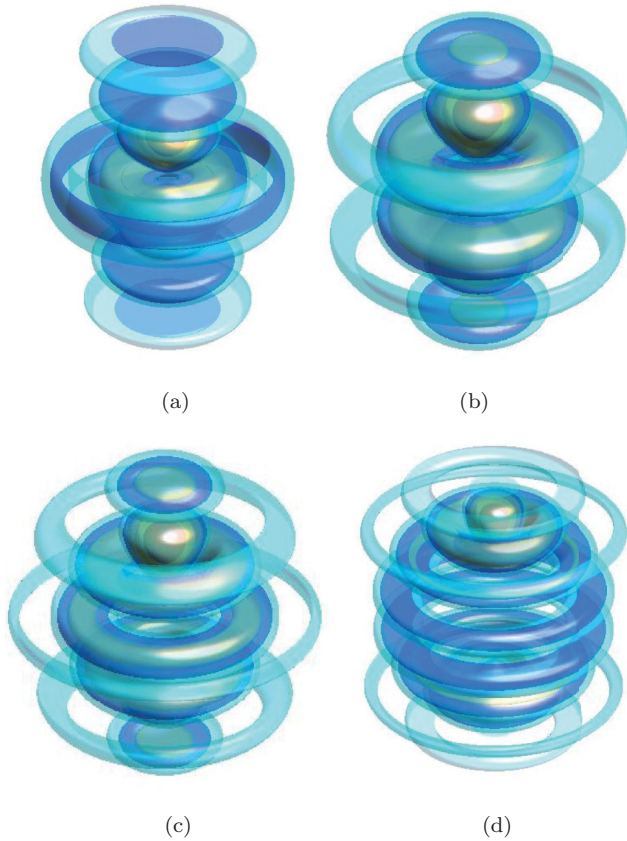(a)   (b)

(c)   (d)

FIG. 3. (Color online) Intensity isosurfaces corresponding to higher order localized waves having $m = 0$ when (a) $\ell = 2$, (b) $\ell = 3$, (c) $\ell = 4$, and (d) $\ell = 7$.

these two wave packets exhibit opposite spins, $\pm m$, then the resulting intensity pattern rotates during propagation with period of $Z_0 = 2\pi/|\alpha_2^2 - \alpha_1^2|$. This behavior is illustrated in
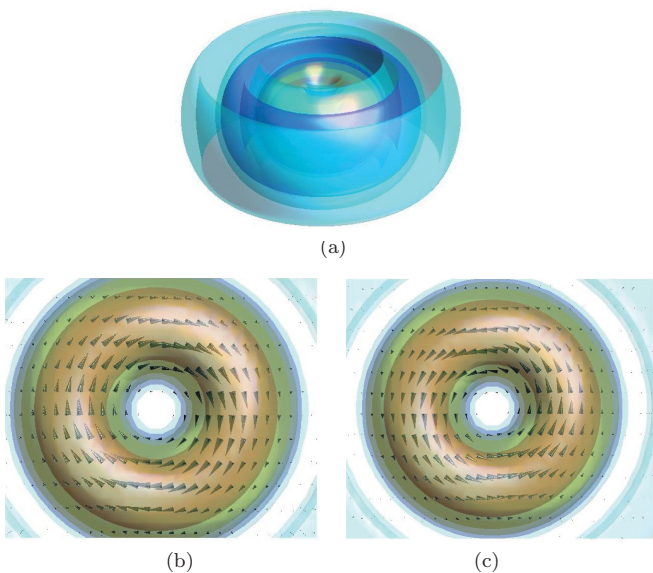

(a)

(b)   (c)

FIG. 4. (Color online) (a) Intensity isosurfaces of an $\ell = 2$; $m = \pm 2$ localized wave. (b) Top view of power circulation when $m = +2$. (c) Power circulation in this same state when $m = -2$.
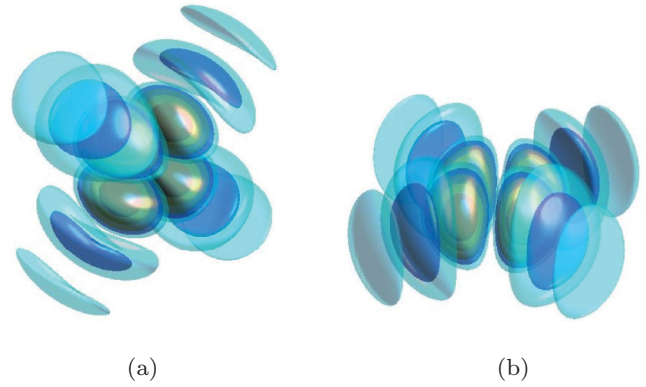

(a)   (b)

FIG. 5. (Color online) Superimposing localized waves with $\ell = 2$; $m = \pm m_0$. (a) Intensity isosurfaces with $m_0 = 1$. (b) Isosurfaces with $m_0 = 2$.

Fig. 6 where a spinning localized wave was generated with two almost degenerate states having $\ell = 2$, $m = \pm 2$, and $\alpha_1 \approx \alpha_2$.

IV. PROPAGATION DYNAMICS OF ENERGY APODIZED LOCALIZED WAVES

It is straightforward to show that the localized waves presented in this paper carry infinite energy. In other words, these spatiotemporal waves happen to be dispersion-diffraction free because they are associated with an infinite norm (very much like plane waves). In practice, any localized wave can only involve finite energy. As a result, it is important to study the dynamics of this family of optical waves when they are appropriately apodized since it is necessary for their generation. In this case, a truncated localized wave is expected to eventually expand in space and time depending on the degree of the apodization itself. Nevertheless, the bigger the space-time aperture, the longer these localized waves will maintain their features and the slower they will deteriorate or expand. In this section, we assume that the apodization is carried out in a Gaussian fashion [3,29]. To analyze these dynamics, we recall that in all cases the electric-field envelope obeys Eq. (2). We also note that in 3D a Gaussian wave packet of the form $G(X, Y, T; Z = 0) = \exp(-R^2/w^2)$ satisfies Eq. (2) and
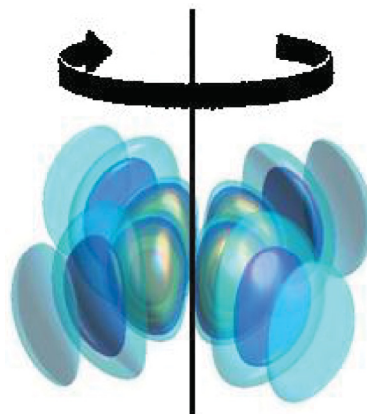

FIG. 6. (Color online) A rotating localized wave.

evolves according to the analytical solution:

$$G(X,Y,T;Z) = \frac{1}{\mu^{3/2}(Z)} \exp\left(-\frac{X^2 + Y^2 + T^2}{w^2\mu(Z)}\right), \quad (13)$$

where $\mu(Z) = 1 + 4iZ/w^2$. Let us now assume that a certain envelope, $\tilde{\psi}(X,Y,T;Z)$, satisfies Eq. (2). In that case, it is straightforward to show that its Gaussian apodized counterpart also satisfies Eq. (2); that is,

$$\psi(X,Y,T;Z) = \frac{1}{\mu^{3/2}(Z)} \exp\left(\frac{-R^2}{w^2\mu(Z)}\right) \tilde{\psi}(\tilde{X},\tilde{Y},\tilde{T};\tilde{Z}),$$
$$(14)$$

where the new coordinates appearing in Eq. (14) have been renormalized with respect to $\mu(Z)$, i.e., $(\tilde{X},\tilde{Y},\tilde{T},\tilde{Z}) = (X,Y,T,Z)/\mu(Z)$. Equation (14) is general and holds in all cases. In the specific case of the apodized localized waves discussed here, (14) leads to

$$\psi = \frac{1}{\mu^{3/2}(Z)} \exp\left(\frac{-R^2}{w^2\mu(Z)}\right) \psi_0 \sqrt{2\pi}\, j_\ell(\alpha\tilde{R}) P_\ell^m(\cos\tilde{\theta})$$
$$\times \exp[im\tilde{\phi}] \exp[-i\alpha^2\tilde{Z}], \quad (15)$$

where the spherical coordinates $(\tilde{R},\tilde{\theta},\tilde{\phi})$ are associated with the coordinates $(\tilde{X},\tilde{Y},\tilde{T};\tilde{Z})$ and are given by the relations $\tilde{R} = R/\mu(Z)$, $\tilde{\theta} = \theta$, and $\tilde{\phi} = \phi$. Figure 7 displays a $Y = 0$ intensity cross section at different diffraction lengths for Eq. (15) with $\ell = 2$, $m = 0$, $\alpha = 1$, $\psi_0 = 1$, and $w = 2$.

As Fig. 7 clearly indicates, the apodized wave packet eventually expands during propagation. This expansion can of course be slowed down by increasing the Gaussian apodization width, w.

## V. LOCALIZED WAVES RESULTING FROM A SPHERICAL SUPERPOSITION ON ARCHIMEDEAN AND PLATONIC SOLIDS

In general, any nonspreading spatiotemporal wave packet can be synthesized through a suitable superposition of "plane-wave solutions" in the normalized $K_X, K_Y, \bar{\Omega}$ space as long as these points lie on a sphere (where in this last expression $\bar{\Omega} = \Omega\tau_0$). This can be understood from Eq. (2), by adopting invariant solutions of the form $\psi = \exp(-i\alpha^2 Z) \exp[i(K_X X + K_Y Y - \bar{\Omega}T)]$. For this case $K_X^2 + K_Y^2 + \bar{\Omega}^2 = \alpha^2$, i.e., the K_X, K_Y, and $\bar{\Omega}$ points should indeed lie on a sphere of radius α. Therefore, any superposition of such plane-wave solutions will also remain invariant as long as they share the same sphere of radius α in reciprocal space. Following this approach, infinitely many realizations of such invariant localized waves are attainable. One such possibility is to consider polyhedra that happen to be inscribable on a sphere such as the Platonic or Archimedean solids. In this case, the field envelope of the localized wave resulting from this superposition can be obtained by

$$\psi_B = \exp(-i\alpha^2 Z) \sum_j \exp(i\vec{Q}_j \cdot \vec{R}), \quad (16)$$
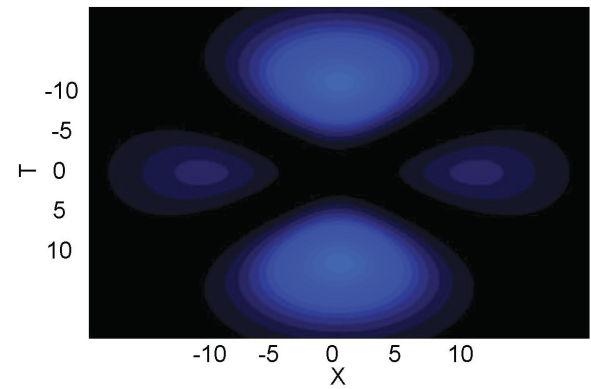
where $\vec{Q}_j$ represents the reciprocal vertices $\vec{Q} = (K_X, K_Y, -\bar{\Omega})$ on this sphere. Figure 8(a) displays the vertices of
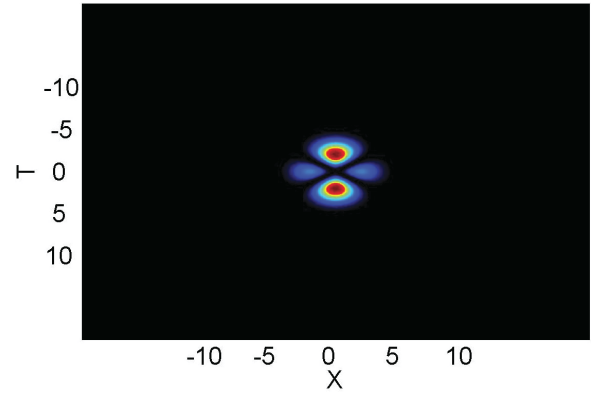
(a)
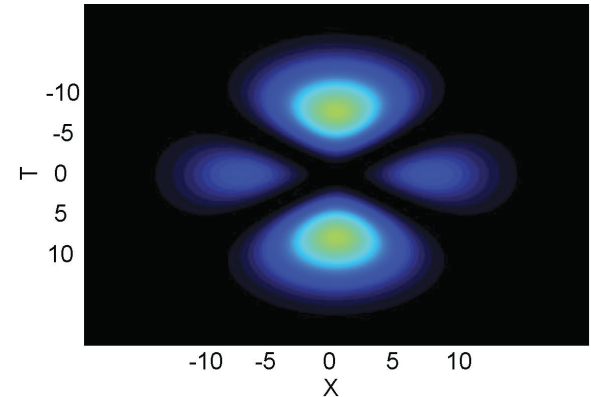
(b)

(c)

FIG. 7. (Color online) Propagation dynamics of an apodized localized wave with $\ell = 2$; $m = 0$ after a normalized distance of (a) $Z = 0$, (b) $Z = 2.66$, and (c) $Z = 4$. Values are normalized to the maximum value of the wave which occurs at $Z = 0$.

a Platonic regular hexahedron on a reciprocal space unit sphere occupying the sites $(\pm 1/\sqrt{3}, \pm 1/\sqrt{3}, \pm 1/\sqrt{3})$. Similarly, the vertices corresponding to an octahedron and dodecahedron are depicted in Figs. 8(b) and 8(c). The respective isointensity plots of the spatiotemporal wave packets that are generated from these three polyhedra are shown in Figs. 8(d)–8(f).
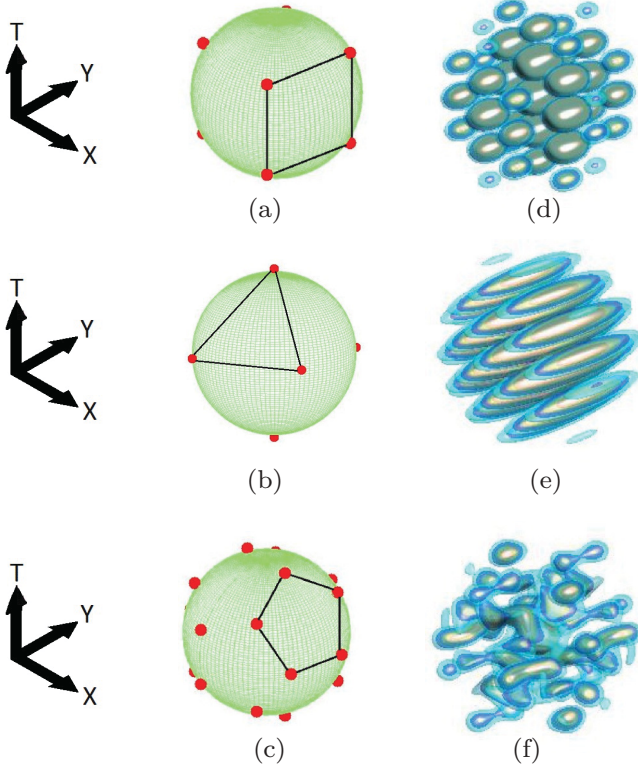
FIG. 8. (Color online) The vertices of a (a) regular hexahedron, (b) octahedron, and (c) dodecahedron inscribed in a Q sphere. (d)–(f) The corresponding isointensity patterns generated from these arrangements.

VI. FOURIER SPECTRA OF APODIZED SPATIOTEMPORAL LOCALIZED WAVES

Fourier spectra provide valuable physical insight not only about the structure of diffraction-dispersion-free waves, but also dictate the requirements concerning their realization in laboratory experiments. In this section, we provide a general analytical expression for the Fourier spectrum of a Gaussian apodized spatiotemporal wave packet that obeys (2). More specifically we obtain the spectrum at the origin $Z = 0$, in which case the initial field envelope is given by $\psi(X,Y,T,Z = 0) = \psi_B(X,Y,T, Z = 0)\exp(-R^2/w^2)$. In general, a nonspreading spatiotemporal wave packet can be described as a Fourier superposition of plane waves in spherical coordinates. Note that in a spherical reciprocal space, $K_X = K_R \sin\theta \cos\phi$, $K_Y = K_R \sin\theta \sin\phi$, and $\bar\Omega = -K_R \cos\theta$. In addition, in this same domain, the spatiotemporal frequencies of a nonspreading wave packet satisfying (2) lie on the surface of a sphere, $K_X^2 + K_Y^2 + \bar\Omega^2 = \alpha^2$, hence its spectrum can be described through the general function $\delta(K_R - \alpha)\zeta(\phi,\theta)$. In this case,

$$
\psi_B(X,Y,T;Z=0) = \frac{1}{(2\pi)^3} \int_0^\infty \int_0^\pi \int_0^{2\pi} dK_R\, d\phi\, d\theta
$$
$$
\times \left[K_R^2 \sin\theta\, \delta(K_R - \alpha)\zeta(\phi,\theta) \right]
$$
$$
\times \exp(i K_R[X \cos\phi \sin\theta
$$
$$
+ Y \sin\phi \sin\theta + T \cos\theta]). \quad (17)
$$

Thus,

$$
\psi_B(X,Y,T;Z=0)
$$
$$
= \frac{1}{(2\pi)^3} \int_0^{2\pi} d\phi \int_0^\pi d\theta [\zeta(\phi,\theta)\alpha^2 \sin\theta]
$$
$$
\times \exp(i\alpha[X \cos\phi \sin\theta + Y \sin\phi \sin\theta + T \cos\theta]). \quad (18)
$$

Given that this localized wave of (18) is apodized in a Gaussian fashion with width, w, its Fourier transform can be obtained from

$$
\Psi(K_X,K_Y,\bar\Omega)
$$
$$
= \int_{-\infty}^\infty \int_{-\infty}^\infty \int_{-\infty}^\infty dX\, dY\, dT\, \exp\left(-\frac{X^2+Y^2+T^2}{w^2} \right)
$$
$$
\times \psi_B(X,Y,T;Z=0) \exp[-i(K_X X + K_Y Y - \bar\Omega T)]. \quad (19)
$$

Upon substituting (18) into (19) for $\psi_B(X,Y,T;Z=0)$, all terms which do not depend on X, Y, or T may be carried out of the Fourier integral. Hence,

$$
\Psi(K_X,K_Y,\bar\Omega)
$$
$$
= \frac{1}{(2\pi)^3} \int_0^{2\pi} d\phi \int_0^\pi d\theta [\zeta(\phi,\theta)\alpha^2 \sin\theta]
$$
$$
\times \int_{-\infty}^\infty \int_{-\infty}^\infty \int_{-\infty}^\infty \exp\left(-\frac{X^2+Y^2+T^2}{w^2} \right)
$$
$$
\times \exp(i\alpha[X \cos\phi \sin\theta + Y \sin\phi \sin\theta + T \cos\theta])
$$
$$
\times \exp[-i(K_X X + K_Y Y - \bar\Omega T)]dX\, dY\, dT, \quad (20)
$$

where now in (20), K_X, K_Y, and $\bar\Omega$ range from $(-\infty,\infty)$. By introducing the auxiliary reciprocal variables $\Xi_X = K_X - \alpha \sin\theta \cos\phi$, $\Xi_Y = K_Y - \alpha \sin\theta \sin\phi$, and $\Xi_T = -\bar\Omega - \alpha \cos\theta$, Eq. (20) becomes

$$
\Psi(K_X,K_Y,\bar\Omega)
$$
$$
= \frac{1}{(2\pi)^3} \int_0^{2\pi} d\phi \int_0^\pi d\theta [\zeta(\phi,\theta)\alpha^2 \sin\theta]
$$
$$
\times \int_{-\infty}^\infty \int_{-\infty}^\infty \int_{-\infty}^\infty \exp\left(-\frac{X^2+Y^2+T^2}{w^2} \right)
$$
$$
\times \exp[-i(\Xi_X X + \Xi_Y Y + \Xi_T T)]dX\, dY\, dT. \quad (21)
$$

The Fourier integrations in (21) can now be performed and lead to

$$
\Psi(K_X,K_Y,\bar\Omega) = \frac{1}{(2\pi)^3} \int_0^{2\pi} d\phi \int_0^\pi d\theta [\zeta(\phi,\theta)\alpha^2 \sin\theta]
$$
$$
\times w^3 \pi^{3/2} \exp\left[-\frac{w^2}{4}\left(\Xi_X^2 + \Xi_Y^2 + \Xi_T^2 \right) \right]. \quad (22)
$$

Substituting the original expressions for the auxiliary parameters Ξ_X, Ξ_Y, and Ξ_T, Eq. (22) can be rewritten as
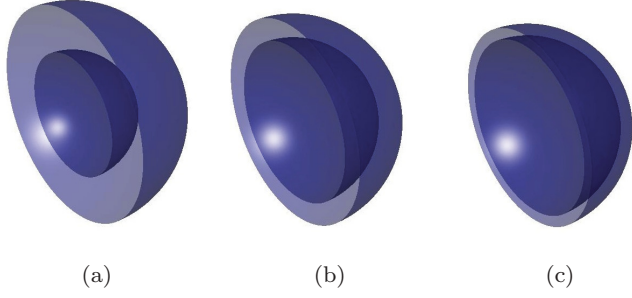
FIG. 9. (Color online) Isosurface spectrum plots of the $\ell = m = 0$ localized wave with various degrees of Gaussian apodization. The spherical spectrum has been sectioned in half so that the shell thickness can be viewed. (a) $w = 5$. (b) $w = 10$. (c) $w = 20$. In the limit that $w \to \infty$, the shell thickness becomes infinitesimally small, representing the spectrum of the O wave.

follows:

$$\Psi(K_X, K_Y, \bar{\Omega}) = \frac{w^3 \pi^{3/2} e^{-(w^2/4)(\alpha^2 + K_X^2 + K_Y^2 + \bar{\Omega}^2)}}{(2\pi)^3}$$
$$\times \int_0^{2\pi} d\phi \int_0^{\pi} d\theta [\zeta(\phi,\theta)\alpha^2 \sin\theta]$$
$$\times \exp\left[i\alpha\left(\frac{w^2}{2i}\right)(K_X \cos\phi \sin\theta\right.$$
$$\left. + K_Y \sin\phi \sin\theta - \bar{\Omega}\cos\theta)\right]. \quad (23)$$

From (23) and (18), one finally obtains the Fourier spectrum of these apodized waves, which is simply given in terms of their original envelope ψ_B, where $[X, Y, T] \to (\frac{w^2}{2i})[K_X, K_Y, -\bar{\Omega}]$. Therefore, the end result is

$$\Psi(K_X, K_Y, \bar{\Omega}) = (\pi w^2)^{3/2} e^{-(w^2/4)(\alpha^2 + K_X^2 + K_Y^2 + \bar{\Omega}^2)}$$
$$\times \psi_B\left(\frac{w^2}{2i} K_X, \frac{w^2}{2i} K_Y, -\frac{w^2}{2i}\bar{\Omega}\right). \quad (24)$$

Equation (24) states that if an invariant solution to (2) is known, then the Fourier transform of its Gaussian apodized version is immediately known. We now see that the Fourier transforms of all the spherical harmonic localized waves introduced in Sec. III can be readily obtained by combining Eqs. (12) and (24). As an example, consider the simplest of these, for which $\ell = m = 0$, and whose field profile is given by $\psi_0 \sqrt{2\pi} j_0(\alpha R) = \psi_0 \sqrt{2\pi} \sin(\alpha R)/\alpha R$. Using (24) we can immediately obtain the corresponding Gaussian apodized Fourier spectrum:

$$\Psi(K_X, K_Y, \bar{\Omega}) \propto w e^{-(w^2/4)(\alpha^2 + K_R^2)} \frac{\sinh(w^2 \alpha K_R/2)}{\alpha K_R}, \quad (25)$$

where $K_R^2 = K_X^2 + K_Y^2 + \bar{\Omega}^2$. Three reciprocal space isosurfaces for both the $\ell = m = 0$ and $\ell = 1$, $m = 0$ cases are plotted for different degrees of Gaussian apodization (Figs. 9
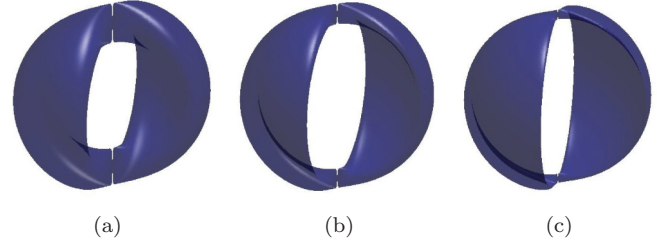

FIG. 10. (Color online) Isosurface spectrum plots of the $\ell = 1$, $m = 0$ localized wave with various degrees of Gaussian apodization. The spherical spectrum has been sectioned in half so that the shell thickness can be viewed. (a) $w = 5$. (b) $w = 10$. (c) $w = 20$.

and 10). As can be seen in Fig. 9, in the limit $w \to \infty$, the thickness of the surfaces becomes infinitesimally small, thus approaching a radius of α. As expected, in this limit the spectrum in Fig. 9 converges to the spectrum of the O wave displayed in Fig. 1. This behavior can be readily understood from Eq. (25). Meanwhile the spectrum of a p_T-like orbital that involves two lobes is displayed in Fig. 10.

VII. CONCLUSIONS

In this paper we have shown that a class of propagation invariant localized waves is possible in anomalously dispersive optical media provided that dispersion and diffraction effects are initially equalized. These field configurations carry spherical harmonic symmetries and can simultaneously negotiate both dispersion and diffraction effects. This offers a robustness that may be exploitable in diverse fields such as microscopy, long-range signal processing, laser femtosecond writing, and laser ablation. The dynamics of such states when they are apodized in a Gaussian fashion was analytically studied along with their associated energy flows. The spectra necessary to generate these waves were analytically obtained. Finally, other types of localized waves generated from Platonic and Archimedean symmetries were examined. In principle, this family of localized waves can also rotate in space-time around a central axis, a feature that could be highly desirable in quasi-nonlinear arrangements as, for example, in beam filamentation studies.

[1] J. Durnin, J. Opt. Soc. Am. A **4**, 651 (1987).

[2] J. J. Durnin, J. J. Miceli, and J. H. Eberly, Phys. Rev. Lett. **58**, 1499 (1987).

[3] J. C. Gutiérrez-Vega, M. D. Iturbe-Castillo, and S. Chávez-Cerda, Opt. Lett. **25**, 1493 (2000).

[4] M. A. Bandres, J. C. Gutiérrez-Vega, and S. Chávez-Cerda, Opt. Lett. **29**, 44 (2004).

[5] J. Y. Lu and J. F. Greenleaf, IEEE Trans. Ultrason. Ferroelectr. Freq. Control **39**, 19 (1992).

[6] D. N. Christodoulides, N. K. Efremidis, P. D. Trapani, and B. A. Malomed, Opt. Lett. **29**, 1446 (2004).

[7] O. Manela, M. Segev, and D. N. Christodoulides, Opt. Lett. **30**, 2611 (2005).

[8] G. A. Siviloglou, J. Broky, A. Dogariu, and D. N. Christodoulides, Phys. Rev. Lett. **99**, 213901 (2007).

[9] G. A. Siviloglou and D. N. Christodoulides, Opt. Lett. **32**, 979 (2007).

[10] H. E. Hernandez-Figueroa, M. Zamboni-Rached, and E. Recami, *Localized Waves* (Wiley Interscience, New Jersey, 2008).

[11] V. Garcés-Chávez, D. McGloin, H. Melville, W. Sibbett, and K. Dholakia, Nature (London) **419**, 145 (2002).

[12] J. Baumgartl, M. Mazilu, and K. Dholakia, Nature Photon. **2**, 675 (2008).

[13] P. Polynkin, M. Kolesik, J. V. Moloney, G. A. Siviloglou, and D. N. Christodoulides, Science **324**, 229 (2009).

[14] G. Milne, K. Dholakia, D. McGloin, K. Volke-Sepulveda, and P. Zemanek, Opt. Express **15**, 13972 (2007).

[15] C. T. A. Brown, D. J. Stevenson, X. Tsampoula, C. McDougall, A. A. Lagatsky, W. Sibbett, F. J. Gunn-Moore, and K. Dholakia, J. Biophotonics **1**, 183 (2008).

[16] B. A. Malomed, D. Mihalache, F. Wise, and L. Torner, J. Opt. B **7**, R53 (2005).

[17] Y. Silberberg, Opt. Lett. **15**, 1282 (1990).

[18] S. Longhi, Opt. Lett. **29**, 147 (2004).

[19] P. Di Trapani, G. Valiulis, A. Piskarskas, O. Jedrkiewicz, J. Trull, C. Conti, and S. Trillo, Phys. Rev. Lett. **91**, 093904 (2003).

[20] M. A. Porras and P. Di Trapani, Phys. Rev. E **69**, 066606 (2004).

[21] H. Sonajalg, M. Ratsep, and P. Saari, Opt. Lett. **22**, 310 (1997).

[22] S. Malaguti, G. Bellanca, and S. Trillo, Opt. Lett. **33**, 1117 (2008).

[23] S. Malaguti and S. Trillo, Phys. Rev. A **79**, 063803 (2009).

[24] A. Chong, W. H. Renninger, D. N. Christodoulides, and F. W. Wise, Nature Photon. **4**, 103 (2010).

[25] X. Liu, L. J. Qian, and F. W. Wise, Phys. Rev. Lett. **82**, 4631 (1999).

[26] M. Dallaire, N. McCarthy, and M. Piché, Opt. Express **17**, 18148 (2009).

[27] S. López-Aguayo, Y. V. Kartashov, V. A. Vysloukh, and L. Torner, Phys. Rev. Lett. **105**, 013902 (2010).

[28] O. V. Borovkova, Y. V. Kartashov, V. E. Lobanov, V. A. Vysloukh, and L. Torner, Opt. Lett. **36**, 2176 (2011).

[29] F. Gori, G. Guattari, and C. Padovani, Opt. Commun. **64**, 491 (1987).